

Electronic Supplementary Material (ESI) for Journal of Materials Chemistry B.

This journal is © The Royal Society of Chemistry 2015

Supporting Information

Design of Versatile Nanocomposite for ‘Seeing’ Drug Release and Action Behavior

Yu Zhang,^[a] Tingting Shen,^[a] Xia Deng,^[b] Yufei Ma,^[c] Lina Wang,^[c] Yong Peng,^[b] Jiang Wu,^[a] Zhijun Zhang,^[c] Weisheng Liu,^[a] and Yu Tang^{*[a]}

^[a] Key Laboratory of Nonferrous Metal Chemistry and Resources Utilization of Gansu Province, State Key Laboratory of Applied Organic Chemistry, College of Chemistry and Chemical Engineering, Lanzhou University, Lanzhou 730000, P.R. China, ^[b] Key Laboratory of Magnetism and Magnetic Materials of Ministry of Education, School of Physical Science and technology, Lanzhou University, Lanzhou 730000, P.R. China, ^[c] Suzhou Institute of Nano-Tech and Nano-Bionics, Chinese Academy of Science, Suzhou 215123, P. R. China

* E-mail: tangyu@lzu.edu.cn

1. Experimental Section

1.1. Materials

1.2. Synthesis of the nanocomposite

1.3. Methods and Instruments

1.4. Experimental Methods

2. Characterization of nanocomposite

2.1. dynamic light scattering (DLS)

2.2. N₂ adsorption-desorption isotherm

2.3. FT-IR spectroscopy

2.4. Magnetization curves

2.5. Schematic illustration and ¹H NMR spectrum of PED

3. Photophysical properties studies

3.1. UV-vis spectra

3.2. Luminescence decay times and emission quantum efficiencies (*Q*)

3.3. PL stability

4. Drug loading and release of nanocomposite

4.1. ¹H NMR, DLS analyses, dye-leaking, and PL spectra as a function of release time

4.2. M-phMSNs@Eu(DBM)₃(phen)@PED used for IBU release real-time monitoring

5. T₂ weighted MR image of nanocomposite

6. Nanocomposite for atomic-resolution TEM imaging

6.1. Morphological comparison of HeLa cells incubated with the 25 μg ml⁻¹ nanocomposite for 0.5h

6.2. Morphological comparison of HeLa cells incubated with the 25 μg ml⁻¹ nanocomposite for 3h.

6.3. Morphological comparison of HeLa cells incubated with the 25 μg ml⁻¹ nanocomposite for 6h.

6.4. The EDX spectra

6.5. Morphological comparison of HeLa cells incubated with the 25 μg ml⁻¹ different NPs for 6h

7. In-vivo assay

References of S.I.

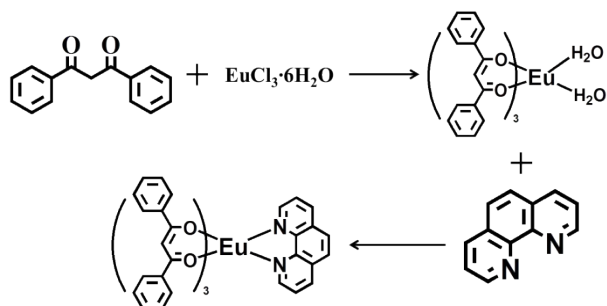
1. Experimental Section

1.1 Materials

Europium chloride ($\text{EuCl}_3 \cdot 6\text{H}_2\text{O}$) were prepared by reacting Eu_2O_3 (99.99%, Shanghai Yuelong) with hydrochloric acid, and then superfluous hydrochloric acid was removed. Tetraethoxysilane (TEOS), oleic acid, oleylamine, iron(III) acetylacetonate ($\text{Fe}(\text{acac})_3$), cetyltrimethylammoniumbromide (CTAB), phenyltriethoxysilane (PTES), octadecyltriethylsilane (C18) and polyethylenimine (PEI) were purchased from J&K Scientific Ltd. Doxorubicin hydrochloride (DOX) was obtained from Beijing Huafeng United Technology Co., Ltd. (Beijing, China). Dibenzoylmethane (DBM) and 1,10-phenanthroline (phen) were purchased from Alfa Aesar and are all analytical reagent (AR). Hoechst 33342 and 4% paraformaldehyde were purchased from Solarbio Co. Ltd..

1.2. Synthesis of the nanocomposite

Synthesis of $\text{Eu}(\text{DBM})_3(\text{phen})$. Solid 1,10-phenanthroline (phen) (18.0 mg, 0.10 mmol) was mixed with 25 mL of 95% ethanolic solution of $\text{Eu}(\text{DBM})_3(\text{H}_2\text{O})_2$ (86.1 mg, 0.30 mmol), and then the suspension was sonicated and filtered. An amount of 25 mL of water was added to the filtrate, following by filtering off the resulting solid (Scheme S1). The pale pink solid was washed with ethanol-water (v/v 1:1) and dried in vacuum at room temperature, obtaining 65.0 mg of $\text{Eu}(\text{DBM})_3(\text{phen})$. Elem. Anal. Calcd: C, 67.98; H, 4.44; N, 2.86; Eu, 15.35. Found: C, 68.12; H, 4.41; N, 2.79; Eu, 15.12.



Scheme S1. Synthesis procedure for the complex $\text{Eu}(\text{DBM})_3(\text{phen})$.

Synthesis of Fe_3O_4 NPs. The Fe_3O_4 nanoparticles were synthesized on the basis of a well-known process.⁵¹ $\text{Fe}(\text{acac})_3$ (0.706 g, 2 mmol) and 1,2-hexadecanediol (2.5845 g, 10 mmol) was dissolved in a mixture of oleic acid (1.9 ml), oleylamine (1.93 ml) and benzyl ether (20 ml). The above mixture solution was heated to 200 °C for 2 h under a flow of nitrogen, and then heated to reflux (~300 °C) and keep at this temperature for 2 h under a blanket of nitrogen. The black-brown mixture was cooled to room temperature by removing the heat source. After addition of 40 ml of ethanol, the black product was precipitated and separated via centrifugation. The black product was dissolved in hexane in the presence of 0.05 ml of oleic acid and 0.05 ml of oleylamine. Centrifugation (6000 rpm, 10 min) was applied to remove any undispersed residue. The product was then precipitated with ethanol, and collected by centrifugation at 8000 rpm. Finally, the product was re-dispersed in hexane.

Synthesis of M-phMSNs. M-phMSNs were prepared by the sol-gel method.⁵² Briefly, 7.5 mg of Fe_3O_4 nanoparticles was dispersed in 1 ml of chloroform, and then was mixed with 10 ml of aqueous solution containing 0.1 g of CTAB under vigorous stirring. The chloroform was evaporated at 65 °C to give the CTAB- Fe_3O_4 dispersion. After addition of 90 ml of distilled water, the mixture was stirred quickly for 2 h at 40 °C. Finally, 3 ml of aqueous ammonia solution (25 wt%), 0.4 ml of TEOS, 0.1 ml of PTES, and 5 ml of ethyl acetate were successively added to the above mixture with rapid stirring for 1 min, and then kept at 80 rpm for another 6 h at 40 °C. The synthesized product was centrifuged, washed with distilled water and ethanol for several times.

In order to load drug molecules into M-phMSNs, further purification through ion exchange was conducted for removal of the structure-directing CTAB. The as-synthesized product was dispersed in a mixture of 40 ml of ethanol and 0.15 ml of concentrated hydrochloric acid. The mixture was refluxed for 24 h, then collected by centrifugation and washed with ethanol repeatedly. Finally, the obtained product dried under vacuum to give the brownish powder.

Modification of the external surface of M-phMSNs with octadecyltriethylsilane (C18) (M-phMSNs@C18). 100 mg of M-phMSNs was first dispersed in 25 ml anhydrous toluene, then 1 ml C18 was added, and the mixture was refluxed for 10 h and collected by centrifugation, washed with ethanol several times, and dried under vacuum. The obtained brownish powder was denoted as M-phMSNs@C18.

Luminescence functionalization of M-phMSNs@C18 by Eu(DBM)₃(phen). 100 mg of M-phMSNs@C18 was dispersed in 10 ml of chloroform, followed by sonication for 30 min. After addition 50 mg of Eu(DBM)₃(phen), the mixture was continuously stirred for 48 h at room temperature followed by filtration and washing with chloroform until no red color emission of the Eu(III) complex was seen from the filtered solution under UV light (365 nm) radiation. The solid was dried at room temperature. And the obtained brownish powder was denoted as M-phMSNs@Eu(DBM)₃(phen).

Synthesis of 4-(dodecyloxy)benzaldehyde (DBD). Anhydrous K₂CO₃ (0.863 g, 33 mmol) was added to 30 ml of CH₃CN, and the solution was degassed with N₂ for 20 minutes. p-Hydroxybenzaldehyde (0.381 g, 27 mmol) was added to the reaction flask, which was heated to 70 °C, following which 1-bromododecane (0.76 ml, 32 mmol) was added. The above solution was refluxed for 12 h, and upon cooling the solvent was removed under reduced pressure. The residue was taken in CH₂Cl₂ (20 ml) and washed with 1 M HCl (10 ml). The organic layer was washed with distilled H₂O (10 ml), and the solvent was removed under reduced pressure and dried by anhydrous MgSO₄ overnight. The crude 4-(dodecyloxy)benzaldehyde (DBD) product was purified by column chromatography (ethyl acetate–petroleum ether, 1:5). ¹H NMR (400 MHz, CDCl₃), δ (ppm): 9.88 (s, 1H, CHO), 7.78 (d, 2H, C₆H₄), 7.32 (d, 2H, C₆H₄), 2.55 (t, 2H, C₆H₄CH₂), 1.63 (m, 2H, C₆H₄CH₂CH₂), 1.26 (m, 18H, CH₂), 0.88 (t, 3H, CH₂CH₃). ESI-MS: [M+H]⁺ m/z 275.3.

Synthesis of PED. 30 mg of DBD was mixed with 500 mg of PEI in 20 ml of ethanol. The mixture was stirred for 24 h at room temperature. Then the product was precipitated by adding hexane, collected by centrifugation at 6000 rpm, and washed with ethanol and hexane (1/5, v/v) for 3 times. The obtained product was denoted as PED.

Drug loading experiment (M-phMSNs@Eu(DBM)₃(phen)-DOX). DOX was dissolved in distilled water with a concentration of 0.5 mg ml⁻¹. 5 mg of M-phMSNs@Eu(DBM)₃(phen) was ultrasonically dispersed in 5 ml of the DOX solution. The mixture was stirred at room temperature for 24 h. Then the dispersion was centrifuged to collect the DOX-loaded nanoparticles and kept the supernatant for calculating the drug loading content. In order to remove the DOX on the exterior surface of nanoparticles, the drug-loaded nanoparticles were washed with distilled water for twice and collected by centrifugation. Finally, the product was dried at 60 °C in vacuum. This product is denoted as M-phMSNs@Eu(DBM)₃(phen)-DOX. The DOX concentration in the supernatant was determined by a UV-Vis spectrophotometer at 480 nm to calculate the drug loading content. The drug loading content and entrapment efficiency were calculated by the following equations: Loading content = (weight of drug in M-phMSNs-DOX)/(weight of M-phMSNs-DOX); Entrapment efficiency = (weight of drug in M-phMSNs-DOX) / (initial weight of drug). DOX encapsulation efficiency was 88.1% and loading content reached up to 8.5%.

Synthesis of PED-coated M-phMSNs@Eu(DBM)₃(phen) and M-phMSNs@Eu(DBM)₃(phen)-DOX. M-phMSNs@Eu(DBM)₃(phen) or M-phMSNs@Eu(DBM)₃(phen)-DOX (10 mg) and PED (20 mg) were dissolved in tetrahydrofuran (1 ml). Then, 5 ml of distilled water was added to this solution with vigorous shaking. The mixture was kept stirring for 24 h at room temperature to evaporate tetrahydrofuran. After that, the product was separated by centrifugation and washed with distilled water several times to remove the unbound copolymer.

The obtained products are denoted as M-phMSNs@Eu(DBM)₃(phen)@PED and the nanocomposite (M-phMSNs@Eu(DBM)₃(phen)-DOX@PED).

1.3. Methods and Instruments

Powder X-ray diffraction (PXRD) patterns were recorded over the 2θ range of 3–65° using a Rigaku-Dmax 2400 diffractometer with Cu K α radiation. Elemental analysis was determined on an ElementarVario EL analyzer. The contents of Eu(III) ions were obtained by inductively coupled plasma-atomic emission spectroscopy (ICP) using an IRIS Advantage ER/S spectrophotometer. Dynamic light scattering (DLS) measurement was conducted on Zetasizer Nanoseries (Nano ZS90). The ¹H NMR spectrum was measured using a Bruker 400 MHz spectrometer in d-trichloromethane with tetramethylsilane [Si(CH₃)₄] as an internal standard. Fourier transform infrared (FTIR) spectra of the materials were conducted within the 4000–400 cm⁻¹ wavenumber range by using a Nicolet 360 FTIR spectrometer with the KBr pellet technique. The luminescent spectrum of drug release was measured in a PBS buffers on a Hitachi F-4500 spectrophotometer. The steady-state luminescence spectra, lifetime measurements, and overall quantum yields of the samples were measured using an Edinburgh Instrument FSL920. The steady-state measurements used a 450W Xe arc lamp as the excitation source and the lifetime used Nd-pumped OPO lette laser as the excitation source. Three parallel measurements were carried out for each sample, so that the presented value corresponds to the arithmetic mean value. The errors in the quantum yield values associated with this technique were estimated to be within 10%. All measurements were carried out at room temperature. The morphological, structural and chemical characterization of all samples were analyzed at the nano/atomic scale using field emission HRTEM (Tecnai™ G2 F30; FEI Company, USA) working at 120 kV, which was equipped with EDX (AMETEK Inc., USA) and high-angle annular dark-field scanning transmission electron microscopy (HAADF-STEM). In the experiments of photoluminescent stability, monochromic light (350 nm) separated from the 450 W Xe arc lamp was used as the irradiation source, with a slit of 0.8 nm and a shutter opening after 10 s for 800 s. The MR imaging experiments in water solutions were performed on a 0.5-T clinical MRI instrument (MesoMR60).

1.4. Experimental Methods

In vitro release. First, nanocomposite (1 mg ml⁻¹) was dispersed in 2 ml of PBS (pH 7.4 and 5.0) and agitated at 300 rpm. The mixture was centrifuged at each hour point. The supernatant (1 ml) was taken for DOX detection and the dye-leaking of Eu(III) complexes measurements, and the same volume of fresh buffer was added back to the residual mixture. The dosing amount of drug was detected by the luminescence intensity of Eu(III) ions of nanocomposite exciting at 400 nm. The amount of released drug in the supernatant was determined by measuring the absorption at 480 nm using a UV-Vis spectrometer. And the dye-leaking of Eu(III) complexes was measured by the luminescence intensity of Eu(III) of supernatant.

Cell culture. HeLa cell lines were provided by the Institute of Biochemistry and Cell Biology, SIBS, CAS (China). Cells were cultured in regular growth medium consisting of RPMI 1640 supplemented with 10 % FBS (fetal bovine serum) at 37 °C in a humidified and 5 % CO₂ incubator. The cells were routinely harvested by treatment with a trypsin-ethylenediaminetetraacetic acid (EDTA) solution (0.25 %).

Cell cytotoxicity assay by MTT protocol. In vitro cytotoxicity was assessed by the standard MTT assay. The statistical evaluation of data was performed using a two-tailed unpaired Student's t-test. Each data point is represented as mean \pm standard deviation (SD) of eight independent experiments ($n = 6$, n indicates the number of wells in a plate for each experimental condition). The dose dependence of the cytotoxicity was investigated at different particle concentrations. HeLa cells were seeded in a 96-well plate at a density of 10⁵ cells per well and cultured in 5 % CO₂ at 37 °C for 24 h. Then, nanocomposite was added to the medium. The cells were incubated in 5 % CO₂ at 37 °C for 24 h. At the end of the incubation, the medium was removed, and 100 μ l of MTT solution (diluted in a culture media with a final concentration of 0.5 mg ml⁻¹) was added and incubated for another 4 h.

The medium was then replaced with 100 μl of dimethyl sulfoxide (DMSO) per well, and the absorbance was monitored using a microplate reader (Bio-TekELx800) at the wavelength of 580 nm. The cytotoxicity was expressed as the percentage of cell viability compared to untreated control cells.

Cellular and nuclear uptake of DOX. Intracellular uptake of DOX was quantified based on the spontaneous fluorescence property of DOX. In brief, HeLa cells were seeded in a 6-well plate, incubated overnight and exposed to 25 $\mu\text{g ml}^{-1}$ DOX or equivalent dose of nanocomposite for 24 h. Then, the cells were washed with PBS three times and trypsinized. After centrifugation, the cell pellet was washed twice with PBS. To separate the cells nuclei from the cell cytosol, the cells were suspended for 10 min at 4 $^{\circ}\text{C}$ in a 100 mM NaCl solution with 1 mM EDTA, 1% Triton X-100, and 10 mM Tris buffer (pH 7.4). The suspension was then centrifuged and the resulting precipitate of cell nuclei was collected. Then 3 ml cell lysis solution (0.5% Triton X-100, 1 M NaOH) was added to disrupt the cells nuclei with ultrasound. Cellular uptake of DOX was then determined by relative fluorescence intensity with excitation at 488 nm and emission at 560 nm.

Cellular DOX quantitation. HeLa cells were incubated with 10 ml of nanocomposite (1 mg ml^{-1}) were added. After 1 h, the cells were washed three times with PBS to remove free nanoparticles. Afterwards, HeLa cells, released by trypsinization as described above, were suspended at a concentration of 10^5 cells/ml for 10 min at 4 $^{\circ}\text{C}$ in a 100 mM NaCl solution with 1 mM EDTA, 1% Triton X-100, and 10 mM Tris buffer solution, and the intensity of Eu(III) were detected by excited at 400 nm. Then the suspension was then centrifuged. Following centrifugation, the supernatant was collected and used for UV-Vis DOX determination.

Magnetic resonance imaging (MRI). The MR imaging experiments were performed on a MesoMR60 0.5-T MR system (Niumag Co. Ltd. shanghai). For the experiments to observe the MR contrast effect of the nanocomposite within the cells, HeLa cells were incubated with nanocomposite for 6 h, and then placed in a 2 ml PCR tube. Each tube contained approximately 10^5 cells.

For T_2 -weighted imaging, the mice were anesthetized using 2% isoflurane (Abbott Laboratories, Abbott Park, IL) mixed with 100% O_2 , which was delivered using a veterinary anesthesia delivery system (ADS 1000; Engler), and then subjected to the nanocomposite (1.0 mg [Fe]/kg) injection. All the nanoparticles were dispersed in PBS buffer, and injected. The contrast signal was obtained using a TurboRARE T_2 pulse sequence: TR/TE/FA, 3000 ms/24 ms/180 $^{\circ}$.

Confocal laser scanning microscopy (CLSM) imaging. For CLSM, the cells were seeded in 12-well culture plates (a clean cover slip was put in each well) and grown overnight as a monolayer. The cells were then incubated with nanocomposite ([DOX] = 25 $\mu\text{g ml}^{-1}$) in 5% CO_2 at 37 $^{\circ}\text{C}$ for 0.5 h, 3 h, 6 h, respectively. Thereafter, the cells were washed with PBS three times, fixed with 2.5 % formaldehyde at 37 $^{\circ}\text{C}$ for 10 min, and then washed with PBS three times again. The cover slips were placed on a glass microscope slide, and the samples were analyzed using CLSM.

Cell transmission electron microscopy (TEM). HeLa cells were cultured with NanoScripts in 12-well culture plates. The cells were then incubated with nanocomposite (the concentration is 25 $\mu\text{g ml}^{-1}$) in 5% CO_2 at 37 $^{\circ}\text{C}$ for 0.5 h, 3 h, 6 h, respectively. The cells were trypsinized and fixed with Trump's Fixative (Electron Microscopy Sciences) for 1 h, washed with sodium cacodylate buffer (Electron Microscopy Sciences), suspended in a 1% osmium tetroxide solution for 1 h, washed with water, and then progressively dehydrated with ethanol (50, 70, 80, 95, 100%). Then the cells were embedded in epoxy resin using the Low Viscosity Embedding Media Spurr's Kit (Electron Microscopy Sciences) following the manufacturer's protocol. The images were obtained with the Tecnai™ G2 F30.

Therapeutic efficacy evaluation of nanocomposite. 4T1 tumor model for therapy evaluation was established by subcutaneously inoculating 4T1 cells ($\sim 8 \times 10^6$) into the nether axillary fossa in the mice. The mice were investigated after 7 days of inoculating. When the tumor was fully developed, the mice were randomly divided into four groups for each group ($n = 6$). 50 μL of PBS, 5 mg kg^{-1} DOX, 50 mg kg^{-1} M-

phMSNs@Eu(DBM)₃(phen)@PED, 50 mg kg⁻¹ nanocomposite (containing 5 mg kg⁻¹ DOX) were intratumoral injected into the mice. The tumor volume and body weight of each mouse were monitored every two days for 16 days. The tumor volume was calculated as length×(width)²×1/2 with a caliper. All the mice were finally sacrificed for further tests. About 0.8 mL of blood from each mouse was collected for blood chemistry tests and complete blood panel analysis before the mouse was euthanized. Major organs from those mice were harvested, fixed in 4% neutral buffered formalin, processed routinely into paraffin, sectioned at 8 mm, stained with hematoxylin and eosin (H&E) and examined under a digital microscope. Statistics were based on standard deviations of 6 mice per group.

2. Characterization of nanocomposite

2.1. Dynamic light scattering (DLS) and powder X-ray diffraction (PXRD) patterns

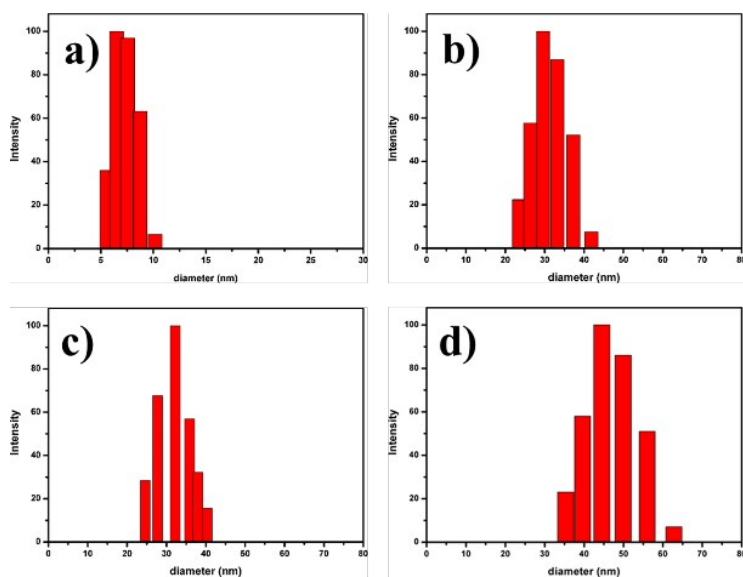


Figure S1. DLS of a) MNPs, b) M-phMSNs, c) M-phMSNs@Eu(DBM)₃(phen), and d) nanocomposite.

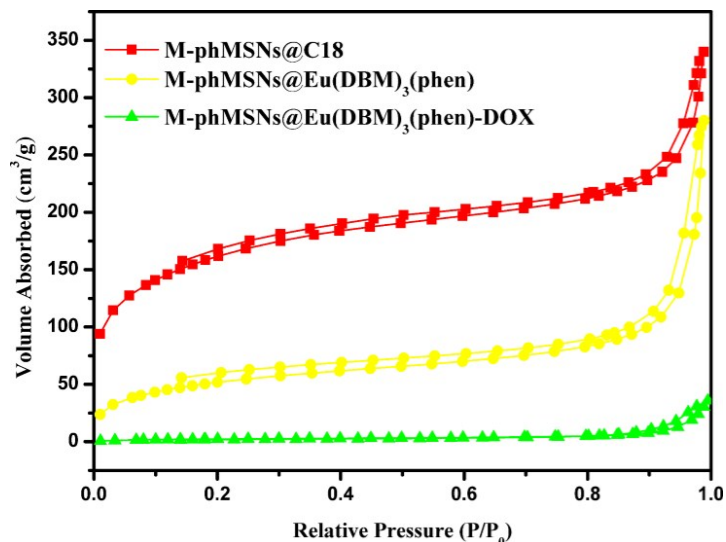
2.2. N₂ adsorption-desorption isotherm

Figure S2. N₂ adsorption-desorption isotherm for M-phMSNs@C18, M-phMSNs@Eu(DBM)₃(phen), and M-phMSNs@Eu(DBM)₃(phen)-DOX.

Table S1. The surface area, pore volume and pore size of M-phMSNs, M-phMSNs@Eu(DBM)₃(phen) and M-phMSNs@Eu(DBM)₃(phen)-DOX.

Samples	BET Surface Area	Pore Volume	Pore Size
	(m ² g ⁻¹)	(cm ³ g ⁻¹)	(nm)
M-phMSNs@C18	542.234	0.526	3.877
M-phMSNs@Eu(DBM) ₃ (phen)	181.294	0.433	2.636
M-phMSNs@Eu(DBM) ₃ (phen)-DOX	8.399	0.0566	0.956

2.3. FT-IR spectroscopy

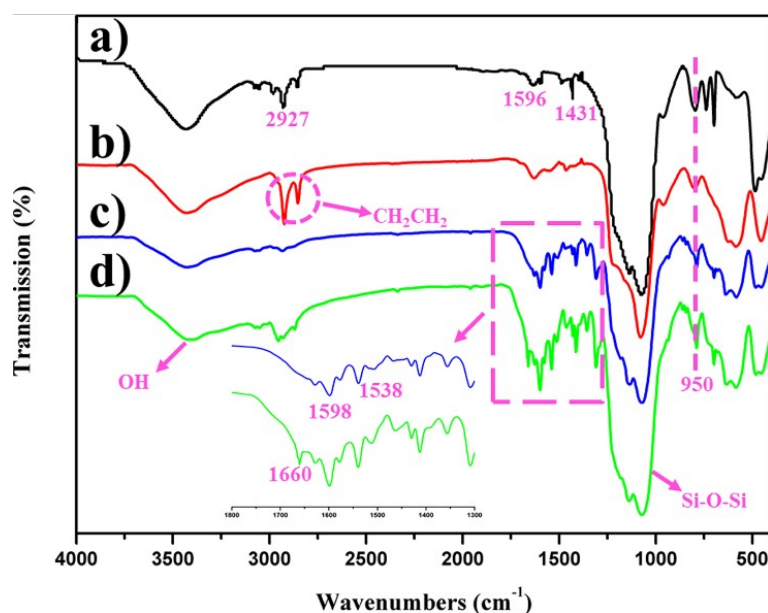


Figure S3. FTIR spectra of a) M-phMSNs, b) M-phMSNs@C18, c) M-phMSNs@Eu(DBM)₃(phen), d) M-phMSNs@Eu(DBM)₃(phen)@PED.

Fourier transform infrared (FTIR) spectra also provided clear evidence for the formation procedure of the multifunctional nanocomposite (Figure S3). As shown in Figure S6a, the Si–OH bond (950 cm⁻¹) in the spectrum of M-phMSNs indicates that a great number of silanol groups exist on the surface of the M-phMSNs for coupling alkyl chains. And the benzene groups (2927 cm⁻¹, 1596 cm⁻¹ and 1431 cm⁻¹) suggested the formation of organic-modified mesoporous silica shell. In the spectrum of M-phMSNs@C18, strong C–H_x bands (2850 cm⁻¹ and 2920 cm⁻¹) suggested the successful conjunction of alkyl chains on the silica (Figure S3b). For the M-phMSNs@Eu(DBM)₃(phen) (Figure S3c), new peaks at 1598 cm⁻¹ and 1538 cm⁻¹ belonging to C=O and C=N appeared according to the spectrum of M-phMSNs@C18, implying that the Eu(DBM)₃(phen) loaded into the nanoparticles successfully. Finally, the prepared ‘door’ PED would associate with the hydrocarbon coupling agents C18 on the surface of M-phMSNs through hydrophobic van der Waals interactions owing to their large number of hydrophobic alkyl chains. As show in Figure S3d, the appearance of characteristic IR peaks at 1640 cm⁻¹ should be attributed to the Schiff base C=N stretching.

2.4. Magnetization curves

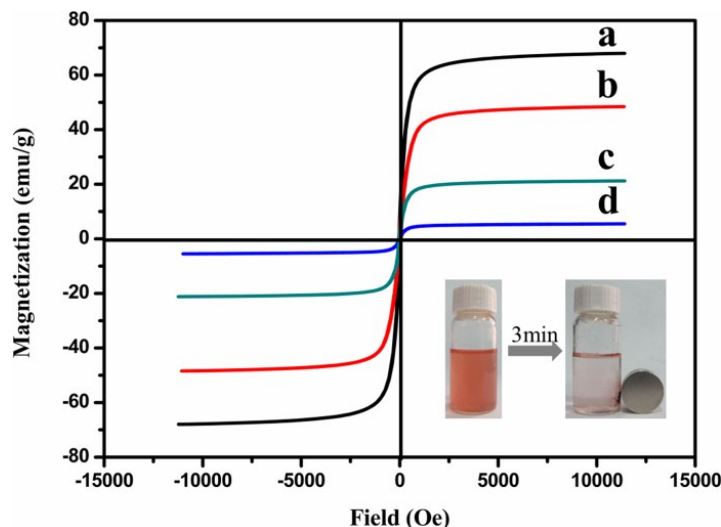


Figure S4. Magnetization curves at room temperature for a) M-phMSNs, b) M-phMSNs@Eu(DBM)₃(phen), c) M-phMSNs@Eu(DBM)₃(phen)-DOX and d) nanocomposite (inset, magnetic targeting under an external magnet).

The magnetic properties of the nanoparticles were studied by a vibrating sample magnetometer (VSM) at 300 K (Figure S4). The magnetization curves show no hysteresis, indicating that all the samples are superparamagnetic at room temperature. The saturation magnetization values for M-phMSNs, M-phMSNs@Eu(DBM)₃(phen), M-phMSNs@Eu(DBM)₃(phen)-DOX, and nanocomposite were 67.59, 48.19, 21.09, and 5.42 emu g⁻¹, respectively. These results indicated that the magnetization of hybrids decreased considerably with the increase of loaded components and PED polymer.^{S3} The magnetic targeting of nanocomposite spheres was tested in PBS solution by placing a magnet close to the glass bottle. The reddish-brown nanocomposite was attracted toward the magnet within a 3 min (inset of Figure S4). Thus this kind of PED-conjugated M-phMSNs mesoporous nanospheres could carry drugs to targeted locations under an external magnetic field.^{S4}

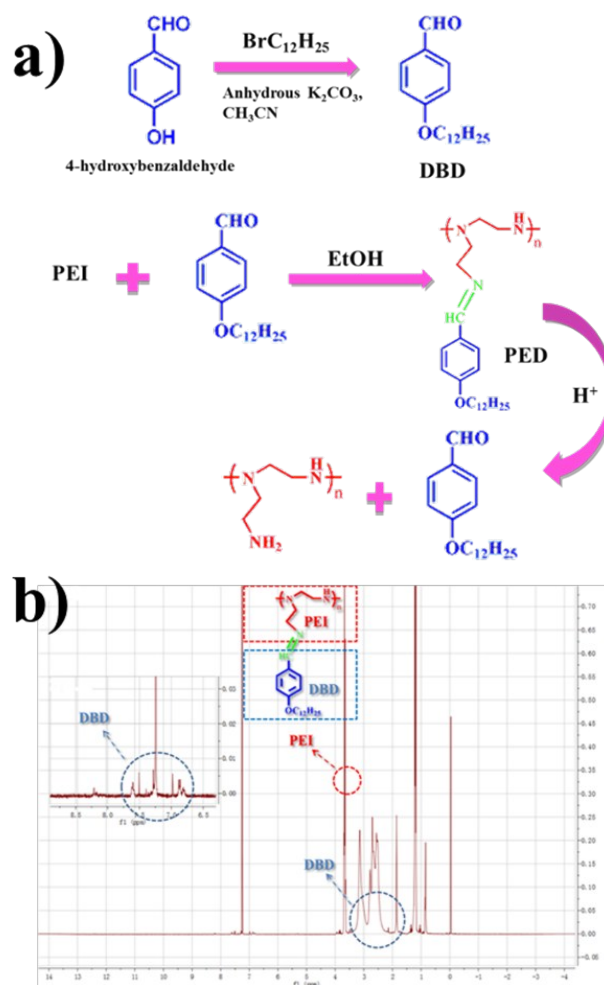
2.5. Schematic illustration and ^1H NMR spectrum of PED

Figure S5. a) Schematic illustration of the synthetic route of PED. b) ^1H NMR spectrum (CDCl_3 , 400MHz) of PED.

Figure S5 shows the synthetic process and ^1H NMR spectrum of PED. The polymer PED was synthesized by polyethylenimine (PEI) and 4-(dodecyloxy)benzaldehyde (DBD). ^1H NMR of PED clearly showed peaks corresponding to DBD besides signals assignable to PEI. These results signified that the structurally well-defined polymer PED was successfully synthesized.

3. Photophysical properties studies

3.1. UV-vis spectra

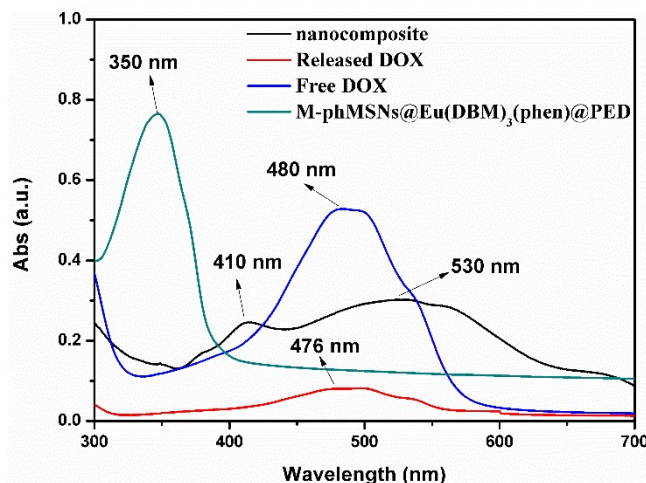


Figure S6. UV-vis spectra of free DOX, M-phMSNs@Eu(DBM)₃(phen)@PED and nanocomposite in PBS buffers (pH = 7.4) at room temperature.

3.2. Luminescence decay times and emission quantum efficiencies (Q)

To further ascertain the coordination effect between DOX and Eu(III) ions, the ⁵D₀ emission decay curves were monitored at 612 nm under the excitation wavelength that maximized the emission intensity. All these curves can be fitted by bi-exponential functions, indicating two kinds of symmetrical site of Eu(III) ion. The fitting data are presented in Table S2, including lifetime values of ⁵D₀ levels of Eu(III) ions, the corresponding relative weightings for each species and the average lifetime $\langle \tau \rangle$. The prolonged lifetimes of M-phMSNs@Eu(DBM)₃(phen)@PED emission (0.279 and 0.578 ms) suggest the super hydrophobic environment in the channel of mesoporous silica shell. Compared to the M-phMSNs@Eu(DBM)₃(phen)@PED, the shortening lifetimes of nanocomposite (0.118 and 0.372 ms) might give rise to the quenching of O-H oscillators from DOX molecule,⁵⁵ which is another evidence for the coordination of DOX to the central Eu(III) ions.

The intrinsic quantum yields (Q_{Ln}) of the hybrid materials containing Eu(III) can be calculated based on the emission spectra and ⁵D₀ lifetimes. The values of Q_{Ln} (%), average lifetimes ($\langle \tau \rangle$), radiative (k_r) and nonradiative (k_{nr}) decay rates for the nanoparticles are shown in Table S2. And the different luminescence lifetimes and quantum yields of these samples are mainly caused by the different environment of the Eu(III) complexes.⁵⁶

The overall luminescence quantum yields $Q_{overall}$ of the samples have been measured by a comparative method.⁵⁷ Quinine sulfate in 0.1M H₂SO₄ (literature quantum yield: 54%) was selected as a standard sample to determine the $Q_{overall}$ of the test samples. The sensitization efficiency of the ligand ($Q_{transfer}$), which reflects the efficacy of excitation energy transfer from ligands to the metal ions, can be calculated.⁵⁸ The commonly accepted mechanism of energy transfer from the organic ligands to the lanthanide ions proceeds through the following steps. At first, the ligands absorb energy via a ground singlet state to the first excited singlet state upon irradiation with ultraviolet radiation. Then, the energy is transferred from the excited singlet state to the triplet state through a nonradiative intersystem crossing process.⁵⁶ When the complexes were doped into the silica channel, the energy transfer efficiency is only 2.58%, possibly due to the energy transfer from the Eu(III) complexes to the phenyl-modified mesoporous channels of M-phMSNs. After DOX introduction into the channels, the energy

transfer efficiency increased to 11.66%, because there is energy transfer from DOX to Eu(III) ions and DOX inhibition to the energy transfer from Eu(III) to M-phMSNs. This result may be attributed to the coordination effect between DOX and Eu(III) ions, which is in agreement with the analyses above.

Assuming that only nonradiative (k_{nr}) and radiative (k_r) processes are involved in the depopulation of the 5D_0 state, Q_{Ln} may be expressed as

$$Q_{Ln} = \frac{k_r}{k_r + k_{nr}} \quad (1)$$

We propose that the average lifetime ($\langle \tau \rangle$), radiative (k_r), and nonradiative (k_{nr}) transition rates may be related through the following equation:

$$k_r + k_{nr} = \langle \tau \rangle \quad (2)$$

The average lifetime $\langle \tau \rangle$ can be calculated using the following equation

$$\langle \tau \rangle = \frac{\sum A_i \tau_i^2}{\sum A_i \tau_i} \quad (3)$$

Where τ_i is the component decay times and A_i is weighed amplitudes.

Quinine sulfate in 0.1M H_2SO_4 (literature quantum yield: 54%) was selected as a standard sample to calculate the $Q_{overall}$ of test samples (i.e. isolated Eu(III) complexes, M-phMSNs@Eu(DBM)₃(phen), and the nanocomposite (M-phMSNs@Eu(DBM)₃(phen)-DOX@PED) which was dissolved in PBS buffers (pH = 7.4) at different concentrations. All the absorbance values of the solutions at the excitation wavelength were measured with UV-Vis spectrophotometer. Photoluminescence (PL) emission spectra of all the sample solutions were recorded by FLS920 Fluorometer under an excitation wavelength of 341 nm. The integrated fluorescence intensity is the area under the PL curve in the wavelength range from 380 to 700 nm. Then a graph was plotted using the integrated fluorescence intensity against the absorbance and a trend line was added for each curve with intercept at zero. The $Q_{overall}$ was calculated using the below equation:

$$Q_x = Q_{ST} \left(\frac{Grad_X}{Grad_{ST}} \right) \left(\frac{\eta_X^2}{\eta_{ST}^2} \right) \quad (4)$$

Where Q_x is the $Q_{overall}$, Grad is the gradient from the plot of integrated fluorescence intensity versus absorbance, and η is the refractive index of the solvent; the subscripts ST and X denote standard and test respectively.

The sensitization efficiency of the ligand ($Q_{transfer}$), which reflects the efficacy with which the ligand transfers its excitation energy to the metal ions, can be calculated as follows:⁵⁸

$$Q_{overall} = Q_{transfer} \times Q_{Ln} \quad (5)$$

Table S2. Photoluminescence data of the isolated Eu(III) complexes, M-phMSNs@Eu(DBM)₃(phen)@PED, and nanocomposite in PBS buffers (pH = 7.4) at room temperature.

	Eu(DBM) ₃ (phen)	M-phMSNs@Eu(DBM) ₃ (phen)@PED	nanocomposite
τ_1 (ms)	0.228 (10.73%)	0.279 (35.86%)	0.118 (9.49%)
τ_2 (ms)	0.396 (89.27%)	0.578 (64.14%)	0.372 (90.51%)
$\langle\tau\rangle$ (ms)	0.378	0.471	0.347
k_r (ms ⁻¹)	0.79	0.929	0.949
k_{nr} (ms ⁻¹)	1.856	1.194	1.933
Q_{Ln} (%)	35.6	43.76	33.02
$Q_{overall}$ (%)	31.39	1.13	3.85
$Q_{transfer}$ (%)	93.42	2.58	11.66

3.3. Time-resolved emission spectra and PL stability

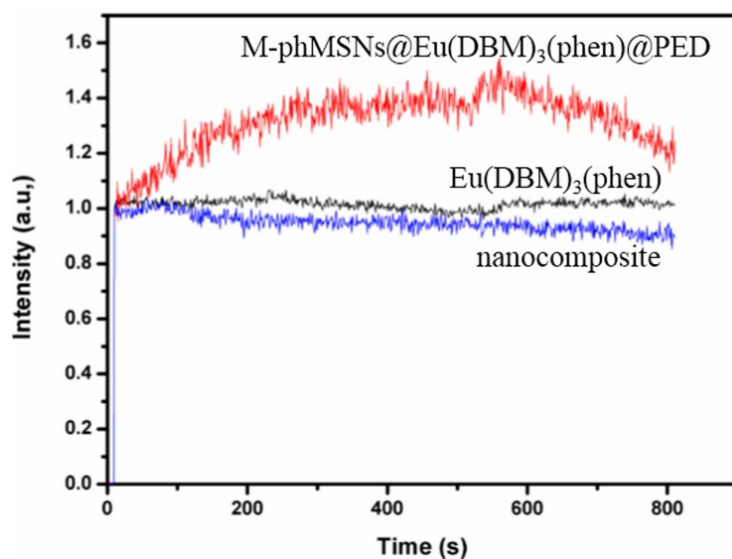


Figure S7. PL stability of the isolated Eu(III) complexes, M-phMSNs@Eu(DBM)₃(phen)@PED, and nanocomposite (normalized intensities of the ⁵D₀→⁷F₂ transition as a function of time) in PBS buffers (pH = 7.4) at room temperature.

For conventional organic fluorophores, two primary drawbacks are the poor photostability and chemical stability. Intriguingly, the fluorescence intensity of M-phMSNs@Eu(DBM)₃(phen)@PED increases with increasing exposure time (Figure S7). These facts suggest that the photostability of Eu(III) complexes has been improved due to the super hydrophobic environment in the channel. In addition, nanocomposite exhibited no drop in fluorescent intensity under increasing exposure time by UV light (350 nm) (Figure S7, blue line). The excellent photostability of nanocomposite indicates that this system can be used to monitor the release of DOX.

4. Drug loading and release of nanocomposite

4.1. ¹H NMR, DLS analyses, dye-leaking, and PL spectra as a function of release time

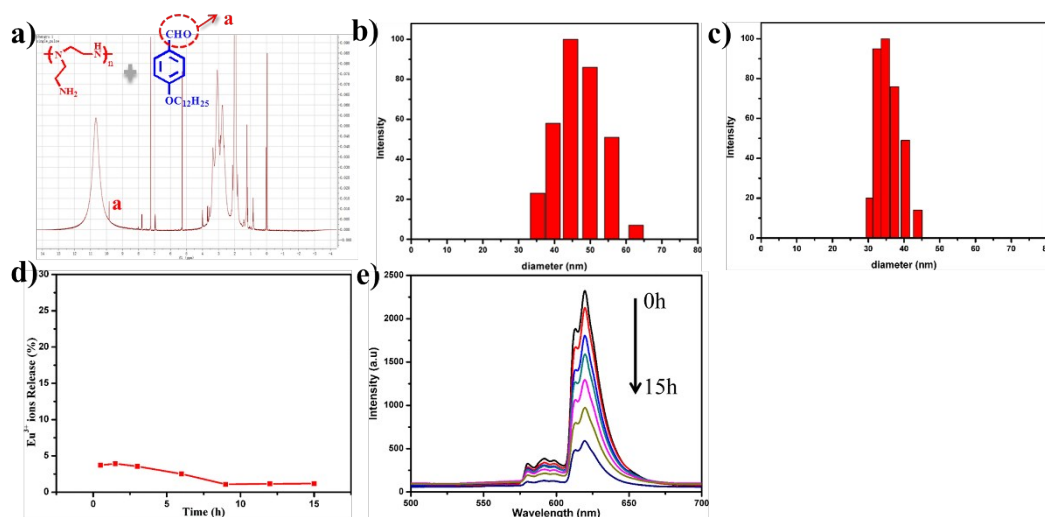


Figure S8. a) ¹H NMR spectrum (CDCl₃, 400MHz) of PED after degradation at pH 5.0. DLS of nanocomposite before b) and after c) the PED hydrolysis. d) The dye-leaking of Eu(III) complexes as a function of release time at 37°C under pH 5.0 which determined from luminescence intensity of the signals at 611 nm. e) Changes in PL emission spectra of nanocomposite as a function of release time at 37°C under pH 5.0.

4.2. M-phMSNs@Eu(DBM)₃(phen)@PED used for IBU release real-time monitoring

The excitation (left) and emission (right) spectra of M-phMSNs@Eu(DBM)₃(phen)@PED and M-phMSNs@Eu(DBM)₃(phen)-IBU@PED in PBS buffers (pH = 7.4) at room temperature are illustrated in Figure S11a and S11b. It can be seen from Figure S9a and Figure S9b that the excitation peak shifted from 379 nm to 304 nm and the excitation peak intensity increased sharply when IBU was loaded into the pore. This result may attribute to the coordination effect between IBU with Eu(III) ions. As discussed above, the luminescence intensity of Eu(III) complexes quenches once the IBU releases from the nanoparticles. To demonstrate this, we incubated IBU-loaded M-phMSNs@Eu(DBM)₃(phen)@PED in PBS buffer at pH = 5.0 and measured the luminescence spectra at different time intervals. As shown in Figure S9d, the emission intensity of M-phMSNs@Eu(DBM)₃(phen)-IBU@PED gradually decreased with increasing dialysis time, which indicates that IBU releases out of M-phMSNs@Eu(DBM)₃(phen)-IBU@PED to induce the quenching of Eu(III) complexes. The plot of *I*_{611nm} as a function of dialysis time in Figure S9e shows that the luminescence intensity of Eu(III) ions in M-

phMSNs@Eu(DBM)₃(phen)-IBU@PED decreases with the dialysis time. These results indicate that the luminescence signals of Eu(III) ions are sufficiently sensitive to be used as imaging probes for detecting the controlled drug release. Figure S9f summarizes the results of the validation study. The luminescence signal intensity (y) at 611 nm shows an excellent linear relationship with the amount of released drug (x): $y=1910.152-15.976x$. The above results reveal that the luminescence signal of nanocomposite is a high-performance reporter that can be used to quantitatively measure the amount of different released drug and efficiency in the course of the disease therapy.

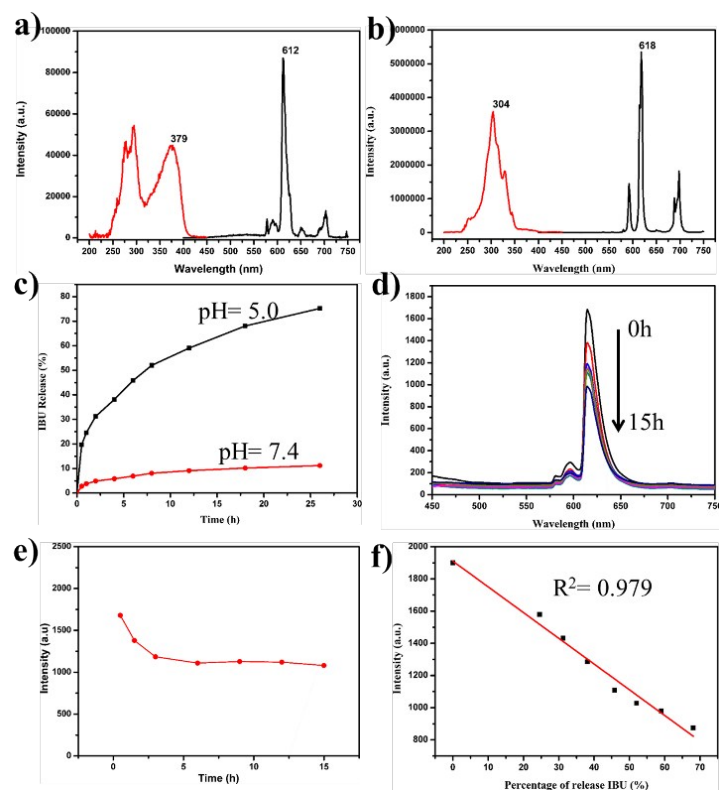


Figure S9. Excitation (red lines, monitored at 612 nm) and emission (black lines, monitored at the maximum excited wavelength which are labeled in the excitation spectra) spectra of a) M-phMSNs@Eu(DBM)₃(phen)@PED and b) M-phMSNs@Eu(DBM)₃(phen)-IBU@PED. c) Release of IBU in vitro from M-phMSNs@Eu(DBM)₃(phen)-IBU@PED at different pH at 37°C. d) Changes in luminescence emission spectra of M-phMSNs@Eu(DBM)₃(phen)-IBU@PED as a function of release time at 37°C under pH=5.0. e) Linear correlation between the released time and the change in the luminescence intensity of the signals at 611 nm. f) Linear correlation between the percentage of IBU released and the change in the luminescence intensity of the signals at 611 nm.

5. T₂ weighted MR image of nanocomposite

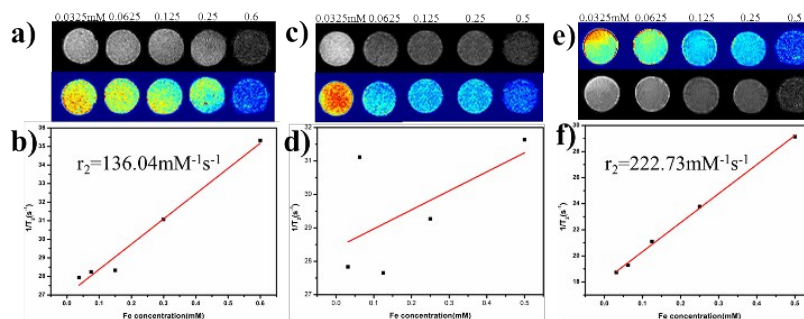


Figure S10. T_2 weighted MR images of a) M-phMSNs and c) M-phMSNs@Eu(DBM)₃(phen)@PED; Plot of T_2^{-1} versus Fe concentration for b) M-phMSNs and d) M-phMSNs@Eu(DBM)₃(phen)@PED. e) T_2 weighted MR images of nanocomposite. f) Plot of T_2^{-1} versus Fe concentration for nanocomposite.

6. Nanocomposite for atomic-resolution TEM imaging

6.1. Morphological comparison of HeLa cells incubated with the 25 $\mu\text{g ml}^{-1}$ nanocomposite for 0.5h

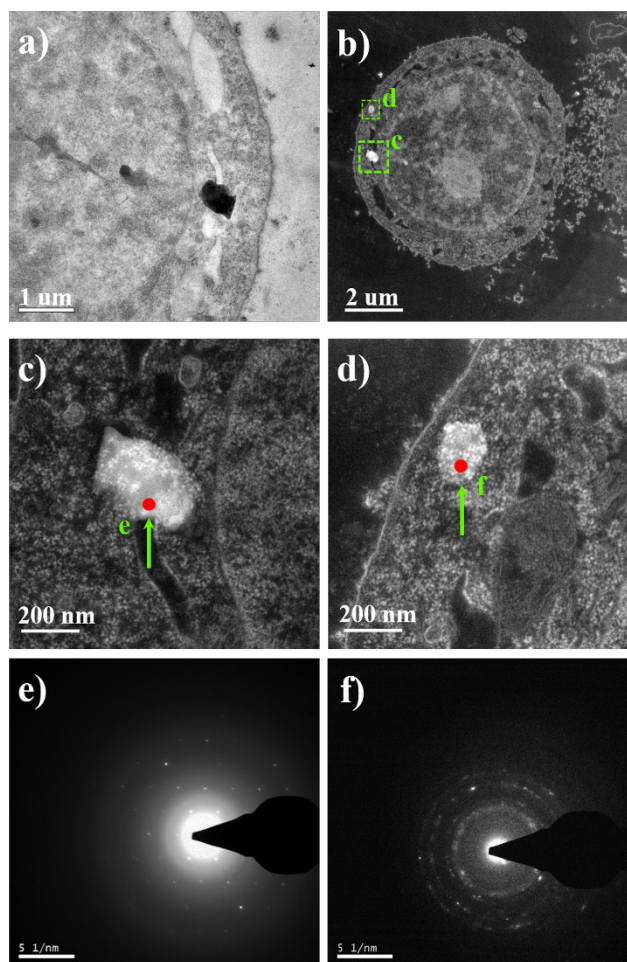


Figure S11. Morphological comparison of HeLa cells incubated with the 25 $\mu\text{g ml}^{-1}$ nanocomposite for 0.5h. a) TEM image of HeLa cells incubated with nanocomposite. b) HAADF-STEM image of an integral HeLa cell incubated with nanocomposite. The bright white contrasts are the aggregated nanocomposite. c) High-magnified image of area c marked by a green square in b. d) High-magnified image of area d marked by a green square in b. e) Convergent beam electron diffraction (CBED) pattern of particle e (red) pointed out by green arrow in c, revealing a clear single crystal structure. f) CBED pattern of particle f (red) pointed out by green arrow in d, revealing a clear single crystal structure.

In order to reveal the intrinsic mechanism of the nanocomposite interacting with individual HeLa cells, we adopted HRTEM, HAADF-STEM and their equipped elemental analysis techniques to investigate the morphology and chemistry of HeLa cells incubated with the nanocomposite. When the HeLa cells were incubated for 0.5 h, the nanocomposite can be found in the cytoplasm in the form of agglomerates (very black crumbs pointed out by

green arrows, Figure S11a). These observations confirm the rapid internalization of the nanocomposite into the cells and subsequent localization in the cytoplasm and subcellular vesicles. And the very black crumbs were identified to be the aggregated nanocomposite by HAADF-STEM (Figure S11b). More images (Figure S11b-d) shows that the large agglomerates of the nanocomposite (bright contrast) can stick onto the cytoplasm and subcellular vesicles. CBED patterns of the nanoparticle images (Figure S11e,f) reveal that the M-phMSNs core of the nanocomposite (red particle E and F pointed out by green arrow in Figure S11c and S11d) remain crystal structure. And the EDX spectra (Figure S14a,b) of the cell area c and d (marked by a green square in Figure S11b) further confirm that the brightly contrasted items were the agglomerates of the nanocomposite.

6.2. Morphological comparison of HeLa cells incubated with the $25 \mu\text{g ml}^{-1}$ nanocomposite for 3h.

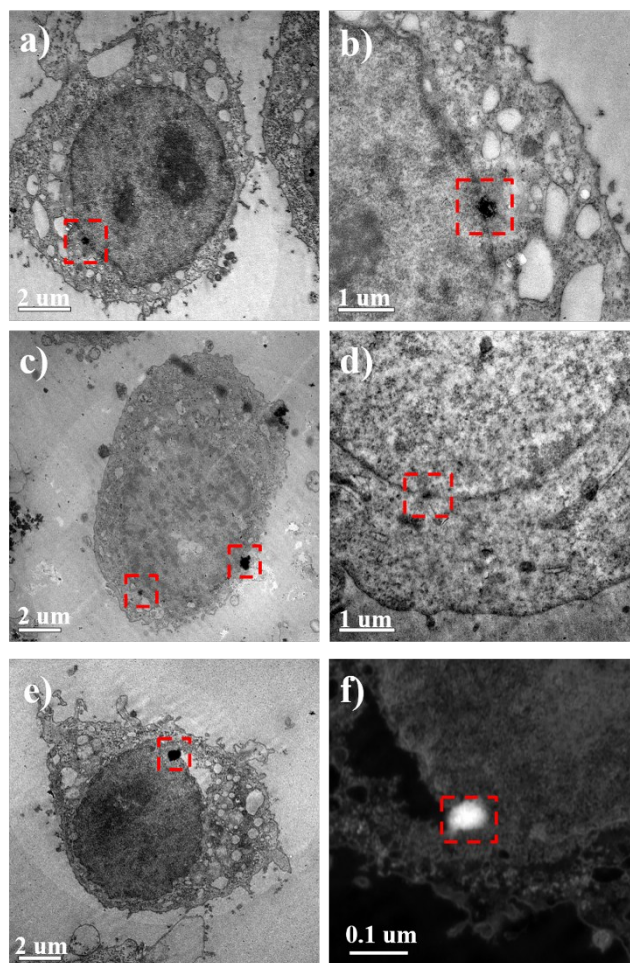


Figure S12. Morphological comparison of HeLa cells incubated with the $25 \mu\text{g ml}^{-1}$ nanocomposite for 3h.

6.3. Morphological comparison of HeLa cells incubated with the $25 \mu\text{g ml}^{-1}$ nanocomposite for 6h.

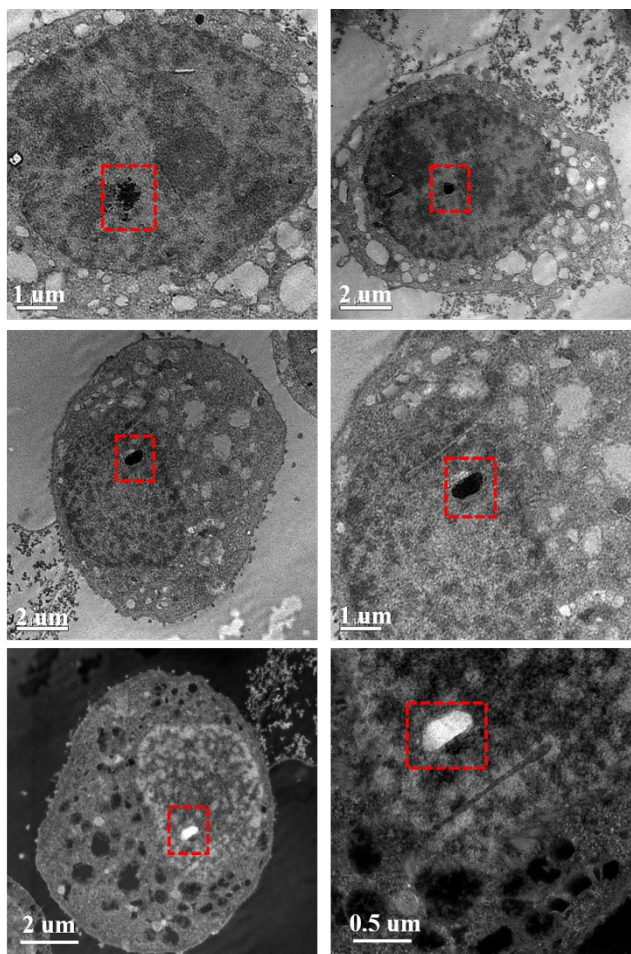


Figure S13. Morphological comparison of HeLa cells incubated with the $25 \mu\text{g ml}^{-1}$ nanocomposite for 6h.

6.4. The EDX spectra

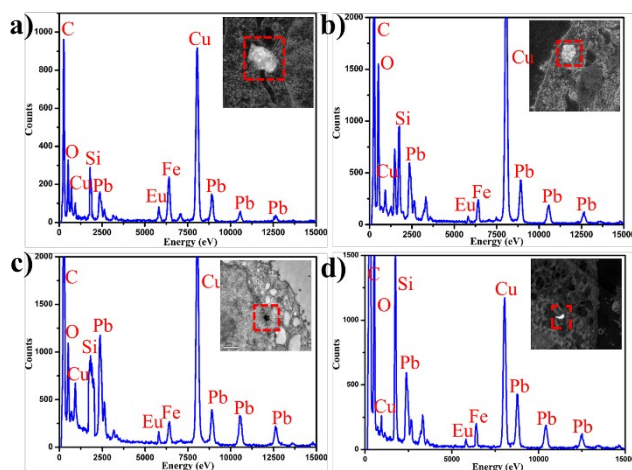


Figure S14. The EDX spectra of a) the nanocomposite from Figure S11c, b) the nanocomposite from Figure S11d, c) the nanocomposite from Figure S12. d) the nanocomposite from Figure 6c.

6.5. Morphological comparison of HeLa cells incubated with the $25 \mu\text{g ml}^{-1}$ different NPs for 6h

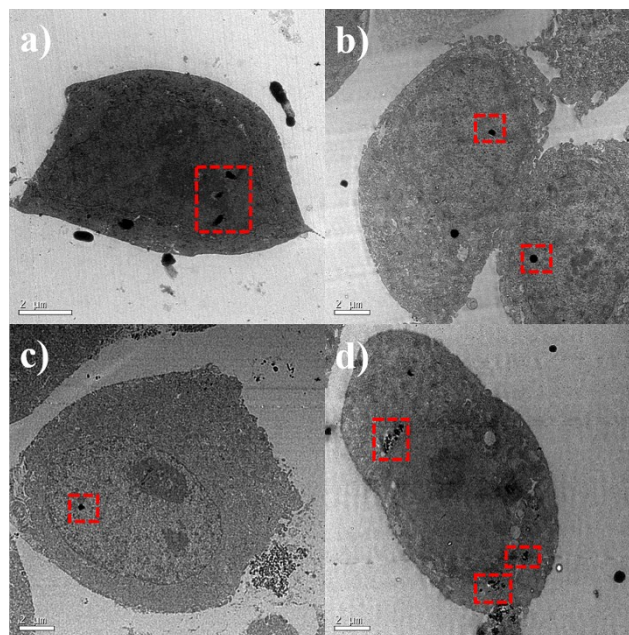


Figure S15. Morphological comparison of HeLa cells incubated with the $25 \mu\text{g ml}^{-1}$ a, M-phMSNs@PED, b, M-phMSNs@Eu(DBM)₃(phen)@PED, c, M-phMSNs@Eu(DBM)₃(phen)-DOX@N-Carboxymethylchitosan-b-DBD and d, M-phMSNs@Eu(DBM)₃(phen)-DOX@P(NIPAm-co-MAA) for 6h.

7. In-vivo assay

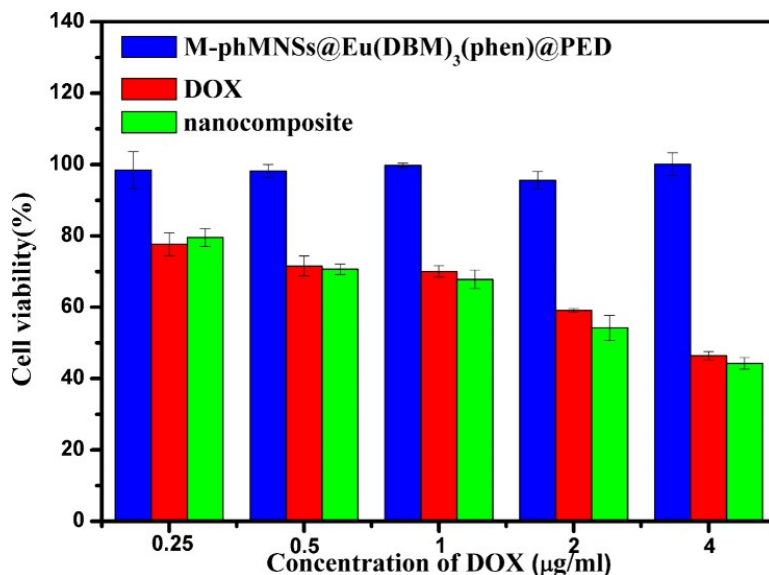


Figure S16. The viability of 4T1 cells with different concentrations of M-phMNSs@Eu(DBM)₃(phen)@PED, nanocomposite and free DOX for 24 h.

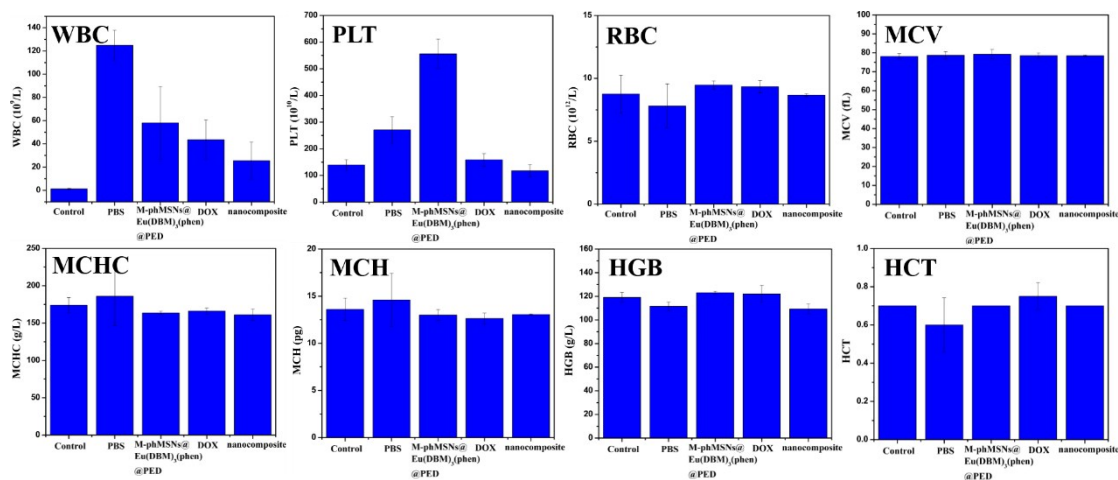


Figure S17. Hematology results of the PBS, M-phMNSs@Eu(DBM)₃(phen)@PED, nanocomposite and free DOX treated mice. These results show mean and standard deviation of white blood cells (WBC), red blood cells (RBC), hematocrit (HCT), mean corpuscular volume (MCV), hemoglobin (HGB), platelets (PLT), mean corpuscular hemoglobin (MCH), and mean corpuscular hemoglobin concentration (MCHC). Bars represent mean standard deviation. Values represent means \pm SE, $n = 3$.

Table S3. The influence of M-phMNSs@Eu(DBM)₃(phen)@PED and nanocomposite on liver function after treatment using serum biochemical analysis. Liver function was evaluated with serum levels of alanine aminotransferase (ALT), aspartate aminotransferase (AST), total protein (TP), creatinine (GREA), and albumin (ALB).

Biomarker	PBS	M-phMSNs@Eu(DBM) ₃ (phen)@PED	DOX	nanocomposite
ALT (U/L)	6.21±1.64	16.59±5.03	15.12 ± 5.68	23.53±8.26
AST (U/L)	120.44±22.34	148.56±7.90	136.17 ± 16.46	179.58±55.85
AST/ALT	19.38±3.62	8.95±1.57	9.01 ± 2.90	7.63±6.76
TP (g/L)	74.90 ± 1.00	66.23 ± 3.34	71.23 ± 3.55	67.40 ± 4.95
GREA (g/L)	< 22.00	< 22.00	< 22.00	< 22.00
ALB (U/L)	19.02 ± 0.05	18.50 ± 1.89	18.67 ± 1.20	17.35 ± 0.97

References of S.I.

- S1. S. H. Sun, H. Zeng, B. R. David, R. Simone, M. R. Philip, S. X. Wang and G. X. Li, *J. Am. Chem. Soc.* 2004, **126**, 273-279.
- S2. J. Kim, J. E. Lee, J. W. Lee, J. H. Yu, B. C. Kim, K. An, Y. S. Hwang, C. H. Shin, J. G. Park, J. Kim and T. Hyeon, *J. Am. Chem. Soc.* 2006, **128**, 688-689.
- S3. J. Kim, H. S. Kim, N. Lee, T. Kim, H. Kim, T. Yu, I. C. Song, W. K. Moon and T. Hyeon, *Angew. Chem. Int. Ed.* 2008, **47**, 8438–8441.
- S4. L. Cheng, K. Yang, Y. G. Li, X. Zeng, M. W. Shao, S. T. Lee and Z. Liu, *Biomaterials* 2012, **33**, 2215-2222.
- S5. Y. F. Ma, H. P. Wang, W. S. Liu, Q. Wang, J. Xu and Y. Tang, *J. Phys. Chem. B* 2009, **113**, 14139–14145.
- S6. H. Martinus, V. Werts, Y. Ronald, T. F. Jukes and J. W. Verhoeven, *Phys. Chem. Chem. Phys.* 2002, **4**, 1542
- S7. C. J. Liu, P. Zhang, X. Y. Zhai, F. Tian, W. C. Li, J. H. Yang, Y. Liu, H. B. Wang, W. Wang and W. G. Liu, *Biomaterials* 2012, **33**, 3604-3613.
- S8. M. Xiao and P. R. Selvin, *J. Am. Chem. Soc.* 2001, **123**, 7067-7073.